Molecular Models of Nucleic Acid Triple Helixes. I. DNA and RNA Backbone Complexes

A. R. Srinivasan and Wilma K. Olson*

Contribution from the Department of Chemistry, Wright-Rieman Laboratories, Rutgers, The State University of New Jersey, 610 Taylor Road, Piscataway, New Jersey 08854-8087

Received August 6, 1997

Abstract: Using a constrained molecular modeling method, we have generated DNA (D), RNA (R), and hybrid DNA/RNA triple-helical structures. Starting with the reference frame defined by the X-ray fiber diffraction model of the poly(dT)·poly(dA)+poly(dT) triple helix, where "·" denotes Watson−Crick pairing and "+" indicates Hoogsteen pairing, we have exhaustively sampled the arrangements of the sugar−phosphate backbone that connect adjacent bases on each of the three strands. We focus attention on regular polymer models constructed from conformationally identical repeating units. Structures free of local steric constraints are combined in all possible ways to build short triplexes, and overall triple helix energies are computed under several different dielectric environments. The predicted ordering of Pyr·Pu+Pyr triplex stabilities, D·D+D > D·D+R > D·R+D > D·R+R > R·D+D > R·D+R > R·R+D > R·R+R, agrees qualitatively with measured stabilities of triplexes containing DNA and/or RNA single strands in gel electrophoresis, NMR, X-ray, and thermodynamic studies. The relevance of the computed data to other triple helical simulations is also discussed.

Introduction

Among the special structural features of nucleic acid double helixes are the grooves formed by the antiparallel sugar−phosphate backbones. The cavities created by the grooves play a vital role in the interactions of DNA and RNA with other molecules, including water,[1] drugs,[2] and proteins.[3,4] The grooves also play a crucial role in enhancing interactions with other nucleic acid molecules. The latter interactions, which are sequence-specific in nature, include associations between double helixes and single strands of either DNA or RNA.[5] For example, both polypurine and polypyrimidine sequences interact with the major groove atoms of duplex structures. These interactions are mediated by the formation of specific hydrogen bonds between the bases of the third strand and the purine bases of the duplex. Nucleic acid triple helixes may be either inter- or intramolecular in nature. The first reported triple helix formed by two strands of polyribo(uridylic acid) and one strand of polyribo(adenylic acid) provides an example of an intermolecular complex made up of three separate strands (trimolecular),[6] while so-called H-DNA is an example of an intramolecular triple helix formed within a single closed circular DNA molecule.[7]

In recent years, increasing interest has focused on triple-helical nucleic acids due to their potential biological relevance, as well as their importance in therapeutic, diagnostic, and biotechnological applications. Many groups have studied the thermodynamics of DNA triple helixes,[8−15] finding triplex formation to be less favorable than the formation of the constituent duplex. The hierarchy of relative energetic stabilities of hybrid nucleic acid triplexes containing various combinations of DNA and RNA strands has been examined by quantitative affinity cleavage titrations,[14] comparative electrophoresis and CD studies,[11] and UV absorption spectrophotometry.[15] While there are some discrepancies among the different experimental measurements, all available studies carried out at high salt concentrations (at least 100 mM NaCl) indicate that DNA/RNA hybrid triplexes containing RNA third strands are more stable than the corresponding triplexes containing DNA third strands. This observation has profound implications with regard to the triplex-based applications noted above.

Early X-ray fiber diffraction studies of the poly(dT)·poly(dA)+poly(dT) and poly(rU)·poly(rA)+poly(rU) complexes,[16] where "·" denotes Watson−Crick pairing and "+" indicates Hoogsteen pairing, yielded A-type structural models in which the pyrimidine third strand engaged in Hoogsteen hydrogen-bonding interactions with the purine strand of the Watson−Crick duplex and all sugar residues adopted a $C_{3'}$-endo puckered conformation (with the $C_{3'}$ atom puckered out of the mean plane of the furanose ring in the direction of the base). More recent two-dimensional (2D) NMR studies of short pyrimidine·-

(1) Berman, H. M. *Curr. Opin. Struct. Biol.* **1994**, *4*, 345−350.
(2) Neidle, S. *Biopolymers (Nucleic Acid Sci.)* **1997**, *1*, 105−121.
(3) Phillips, S. E. V.; Moras, D. *Curr. Opin. Struct. Biol.* **1993**, *3*, 1−2.
(4) Suzuki, M.; Yagi, N. *J. Mol. Biol.* **1996**, *255*, 677−687.
(5) Thuong, N. T.; Hélène, C. *Angew. Chem.* **1993**, *32*, 666−690.
(6) Felsenfeld, G.; Davies, D. R.; Rich, A. *J. Am. Chem. Soc.* **1957**, *79*, 2023−2024.
(7) Htun, H.; Dahlberg, J. E. *Science* **1989**, *243*, 1571−1576.
(8) Manzini, G.; Xodo, L. E.; Gasparotto, D.; Quadrifoglio, F.; van der Marel, G. A.; van Boom, J. H. *J. Mol. Biol.* **1990**, *213*, 833−843.
(9) Plum, G. E.; Park, Y.-W.; Singleton, S. F.; Dervan, P. B.; Breslauer, K. J. *Proc. Natl. Acad. Sci. U.S.A.* **1990**, *87*, 9436−9440.
(10) Pilch, D. S.; Levenson, C.; Shafer, R. H. *Biochemistry* **1991**, *30*, 6081−6087.
(11) Roberts, R. W.; Crothers, D. M. *Science* **1992**, *258*, 1463−1466.
(12) Roberts, R. W. Ph.D. Thesis, Yale University, New Haven, CT, 1993.
(13) Park, Y.-W. Ph.D. Thesis, Rutgers University, New Brunswick, NJ, 1992.
(14) Han, H.; Dervan, P. B. *Proc. Natl. Acad. Sci. U.S.A.* **1993**, *90*, 3806−3810.
(15) Escudé, C.; Francois, J.-C.; Sun, J.-S.; Ott, G.; Sprinzl, M.; Garestier, T.; Hélène, C. *Nucleic Acids Res.* **1993**, *21*, 5547−5553.
(16) Arnott, S.; Bond, P. J.; Selsing, E.; Smith, P. J. C. *Nucleic Acids Res.* **1976**, *3*, 2459−2470.

S0002-7863(97)02720-0 CCC: $15.00
Published on Web 01/13/1998

purine+pyrimidine DNA triplexes[17−19] and an ^{15}N NMR analyses of a 21 base pair duplex with a shorter (15 nucleotide) third strand[20] have confirmed the Hoogsteen base pairing scheme proposed by the fiber diffraction model. NMR studies of the $d(TC)_4$·$d(GA)_4$+$d(TC)_4$ triplex[17] and $d(T)_6$·$d(A)_6$+$d(T)_6$[19] indicate mixed results on the preference of sugar puckering in these complexes. Circular dichroism, infrared, and molecular modeling investigations, on the other hand, suggest that DNA triple helixes are members of the B-DNA family of structures, with the sugars of all strands in the $C_{2'}$-endo puckered form.[21,22] It is important to note that a $C_{3'}$-endo to $C_{2'}$-endo sugar repuckering is followed by an ∼1 Å increase in the nonbonded distances between adjacent phosphorus atoms in each single strand and that ring repuckering is sometimes,[23] but not always,[24] tied to a large-scale configurational change from the A- to B-helical form.

X-ray diffraction studies of single crystals of the model triplex, C_3T_{12}·A_{12}+$T_{12}C_3$, and the hetero-oligomer, $C^+TC^+_2T_3$-$C^+T_2C^+_2T$·$GAG_2A_3GA_2G_2T$+$ACTC_2T_3CT_2C_2A$, have yielded only fiber-type diffraction patterns because of lack of ordering.[25] The data, nevertheless, suggest a B-type structure with $C_{2'}$-endo sugar puckering in both triplexes. The triple helix with homo-oligomeric A and T sequences is 13-fold with a rise per residue of 3.26 Å, a structure somewhat different from the classical poly(dT)·poly(dA)+poly(dT) triple-helical structure (12-fold with a rise per residue of 3.26 Å) and the triplex with a hetero sequence (∼12 residues per turn and 3.2 Å rise per residue).

The currently available (NMR and X-ray) structural database of nucleic acid triplexes is thus small. Molecular modeling and dynamics studies[26−28] have helped to fill this gap in knowledge and, at the same time, provide potentially useful insights into the three-dimensional conformations of triple helical complexes. Most of these studies, carried out in the presence of solvent molecules or *in vacuo*, consistently point to a repuckering of the sugar rings in the complex from $C_{3'}$-endo to either $O_{1'}$-endo or $C_{2'}$-endo conformations. (The $O_{1'}$-endo state is commonly thought to be a high-energy intermediate between the $C_{3'}$-endo and $C_{2'}$-endo forms.[29]) The relative proportions of the puckered states, however, vary in different dynamics studies. These preferences apparently reflect the choice of force field, which is known to lead to entirely different predictions in simulations of otherwise identical duplex systems.[30−32] Many published simulations of DNA triplexes ignore long-range electrostatic effects, which can have a substantial effect on the preferred ring conformation (see below). Optimization studies of regular $d(T)_n$·$d(A)_n$+$d(T)_n$ triple-helical structures[21,33] also give conflicting results. Calculations[22,27] based on the JUMNA[34] and AMBER[35] force fields, respectively using the triple helical fiber model and the canonical B- and A-DNA double helixes as starting structures, predict that the purine strand preferentially adopts the $C_{2'}$-endo conformation. Corresponding calculations[36] employing the CHARMM[37] force field, by contrast, indicate a preference for $C_{3'}$-endo sugars in model $d(T)_7$·$d(A)_7$+$d(T)_7$ triple helixes. These differences presumably reflect the built-in preferences of the force fields described above.

In this paper, we report a constrained molecular modeling study of regular DNA, RNA, and DNA/RNA hybrid triple helixes. To our knowledge, no one has yet generalized DNA triplex construction methods for analyses of RNA and hybrid complexes and incorporated all possible combinations of sugar puckering in molecular models. Starting with the Watson−Crick and Hoogsteen base pairing schemes supported by fiber diffraction, single crystal, and NMR studies, we have evaluated all possible combinations of DNA and RNA sugar-phosphate backbones that connect adjacent bases on each of the three strands of the poly(dT)·poly(dA)+poly(dT) triplex. In these cases, we identify the potential polymer building blocks and rank the monomer repeating units according to their conformational energies.

We then generate triple helixes made up of 16 identical monomer repeating units from all possible sets of the low-energy building blocks. We choose this chain length in order to compare our predictions with experiments carried out on triple-helical DNAs of comparable length. The total energies of the different triple helixes are computed using a set of standard potential functions. The effects of counterion condensation as well as different dielectric treatments are considered. The relative energies of DNA, RNA, and mixed DNA/RNA triplexes are compared with observed stabilities derived from gel electrophoresis, NMR, and thermodynamic measurements of the corresponding structures. To estimate the relative deformability of the triplets compared to conventional base-paired duplexes, we also compute the potential energies of interaction of free base pairs in typical helical arrangements.

Methods

Constrained Nucleic Acid Model Building. The different nucleic acid backbone combinations that link a chosen three-dimensional arrangement of bases can be determined by considering the various combinations of sugar and glycosyl geometries that bring the intervening 3′- and 5′-ester oxygens within standard phosphate bonding distances.[38] The glycosyl and sugar torsions (both the ring puckering and the exocyclic $O_{5'}-C_{5'}-C_{4'}-C_{3'}$ torsion termed γ[39]) are treated here as independent variables. When the resulting $O_{3'}\cdots O_{5'}$ distances conform to the known geometry of phosphate chemical bonding,[40] an intervening phosphorus atom with the correct C−O−P

(17) Rajagopal, P.; Feigon, J. *Nature (London)* **1989**, *339*, 637−640.
(18) de los Santos, C.; Rosen, M.; Patel, D. *Biochemistry* **1989**, *28*, 7282−7289.
(19) Umemoto, K.; Sarma, M. H.; Gupta, G.; Luo, J.; Sarma, R. H. *J. Am. Chem. Soc.* **1990**, *112*, 4539−4545.
(20) Gaffney, B. L.; Kung, P.-P.; Wang, C.; Jones, R. A. *J. Am. Chem. Soc.* **1995**, *117*, 12281−12283.
(21) Howard, F. B.; Miles, H. T.; Liu, K.; Frazier, J.; Raghunathan, G.; Sasisekharan, V. *Biochemistry* **1992**, *31*, 10671−10677.
(22) Ouali, M.; Letellier, R.; Adnet, F.; Liquier, J.; Sun, J.-S.; Lavery, R.; Taillandier, E. *Biochemistry* **1993**, *32*, 2098−2103.
(23) Saenger, W. *Principles of Nucleic Acid Structure*; Springer-Verlag: New York, 1984; Chapter 11.
(24) Schneider, B.; Neidle, S.; Berman, H. M. *Biopolymers* **1997**, *42*, 113−124.
(25) Liu, K.; Miles, H. T.; Parris, K. D.; Sasisekharan, V. *Struct. Biol.* **1993**, *1*, 11−12.
(26) Laughton, C. A.; Neidle, S. *J. Chim. Phys.* **1991**, *88*, 2597−2603.
(27) Kiran, M. R.; Bansal, M. *J. Biomol. Struct. Dyn.* **1995**, *13*, 493−505.
(28) Sekharudu, C. Y.; Yathindra, N.; Sundaralingam, M. *J. Biomol. Struct. Dyn.* **1993**, *11*, 225−244.
(29) Olson, W. K. *J. Am. Chem. Soc.* **1982**, *104*, 278−286.
(30) Cheatham, T. E., III; Kollman, P. A. *J. Mol. Biol.* **1996**, *259*, 434−444.
(31) Yang, L.; Pettitt, B. M. *J. Phys. Chem.* **1996**, *100*, 2564−2566.
(32) Feig, M.; Pettitt, B. M. *J. Phys. Chem. B* **1997**, *101*, 7361−7363.
(33) Raghunathan, G.; Miles, H. T.; Sasisekharan, V. *Biochemistry* **1993**, *32*, 455−462.
(34) Lavery, R.; Zakrzewska, K.; Sklenar, H. *Comput. Phys. Commun.* **1995**, *91*, 135−158.
(35) Pearlman, D. A.; Case, D. A.; Caldwell, J. W.; Ross, W. S.; Cheatham, T. E., III; DeBolt, S.; Ferguson, D.; Seibel, G.; Kollman, P. *Comput. Phys. Commun.* **1995**, *91*, 1−41.
(36) Cheng, Y.-K.; Pettitt, B. M. *Biopolymers* **1995**, *35*, 457−473.
(37) MacKerell, J. A. D.; Wiorkiewicz-Kuczera, J.; Karplus, M. *J. Am. Chem. Soc.* **1995**, *117*, 11946−11975.
(38) Srinivasan, A. R.; Olson, W. K. *J. Biomol. Struct. Dyn.* **1987**, *4*, 895−938.

valence angles is located. Four sequential torsion angles about the $C_{4'}-C_{3'}-O_{3'}-P-O_{5'}-C_{5'}-C_{4'}$ bonds are thereby obtained as dependent variables.[38] When the backbone solutions are computed, the sugar puckering in adjacent residues is varied over 20 evenly spaced pseudorotational states (P_1, P_2) of amplitude 38°, while the exocyclic $C_{5'}-C_{4'}$ sugar torsion (γ) and the glycosyl angles (χ_1, χ_2) are varied at 10° increments between 0° and 350°. The hydroxyl of ribose is treated, for simplicity, as a single atom (with reduced charge) in the energy calculations described below.

Modeling Nucleic Acid Triple Helixes. Construction of a feasible triplex model involves the formation of three backbone linkages in the purine and pyrimidine strands of the complex. Starting with the idealized base positioning in the poly(dT)·poly(dA)+poly(dT) fiber diffraction model,[41] we determine all possible polymer building blocks that connect sequential bases on the three strands. The independent parameters are varied over the ranges specified above, but because of the assumed conformational identity of the glycosyl and pseudorotational variables in successive residues, the chain closure search is simplified. The sets of monomer units are then combined to form triple helixes with 16 residues in each single strand, the energy of which (including both intra- and intermolecular interactions of all nonbonded atomic pairs) is assessed with the potential functions and dielectric treatments outlined below.

Potential Energies. The total potential energy V of the triple-helical structures is estimated on the basis of a standard semiempirical potential function[42,43] that accounts for additive contributions arising from nonbonded and torsional terms. The nonbonded contributions V_{nb} are a function of the distance r_{ij} between nonbonded atom pairs (i and j) and are calculated as a sum over all pairwise contributions in the form of van der Waals' and Coulombic interactions ($V_{nb} = V_{vdw} + V_{el}$).

The van der Waals' contributions—a sum of repulsive and attractive terms, V_{vdw}—are estimated by a combination of 6−12 and 10−12 potentials (the latter applied to hydrogen bonds). The electrostatic energy, V_{el}, is assessed with a Coulombic potential. The set of atomic charges for DNA and RNA is derived from very high resolution, single-crystal X-ray diffraction studies of model nucleosides and nucleotides at low temperature.[44] These charges reproduce stacking distances in dimer models of neighboring $(A\cdot T)_2$ and $(G\cdot C)_2$ base pairs (data not shown). Because the bases are fixed in the triplex, it is not necessary to introduce a hydrogen bonding potential.

Explicit modeling of nucleic acid−salt and nucleic acid−solvent interactions, while becoming feasible in representative simulations of short nucleic acid helixes,[30,36,45,46] is out of the question for conformational searches as exhaustive as those carried out here. Our desire to sample conformation space as widely as possible forces us, of necessity, to adopt an implicit representation of the chemical environment. In view of the uncertainties of such an approach, we examine a range of feasible treatments of the energy contributions. The dielectric constant ϵ is assigned a value of 4 in initial calculations at the level of local dimer formation but is considered as a distance-dependent variable in subsequent oligomer models (see below). The influence of the local ionic environment is treated indirectly through reduction of the net charge on the phosphate group by 0.848 esu (i.e., $\delta_{phosphate} = -0.152$ esu),[38] in accordance with the concepts of counterion condensation theory.[47] This is accomplished in the triplex models by modifying the residual charges on the pendent oxygen atoms of the phosphodiester. The level of charge reduction is based on the mean spacing of residues in the standard triple helix and the assumption of condensed monovalent counterions. (The estimated degree of charge condensation per phosphate unit would increase to 0.924 esu if the counterions were divalent.)

The dielectric constant used in the electrostatic calculations of the triple−helical structures is chosen to mimic the long-range screening of charged interactions by solvent. As a first approximation, ϵ is set equal to the dielectric constant of water ($\epsilon_\infty = 78.3$). At the next level of approximation, a standard Debye−Hückel screening term, $\epsilon(r_{ij}) = \epsilon_\infty \exp(r_{ij}/D)$, is used. The parameter D is the Debye length, a constant proportional to the ionic strength and here taken to be 10 Å, corresponding to a salt concentration of ∼0.1 M. Three different sigmoidal dielectric functions are also considered. The first, developed by Hingerty et al.,[48] mimics the binding of selected cations with the crystalline GpC monoanion:

$$\epsilon(r_{ij}) = \epsilon_\infty - (\epsilon_\infty - 1)\left(\frac{r_{ij}}{2.5}\right)^2 \frac{\exp\left(\frac{r_{ij}}{2.5}\right)}{\left(\exp\left(\frac{r_{ij}}{2.5}\right) - 1\right)^2} \qquad (1)$$

The function, introduced by Mazur and Jernigan,[49] which mimics the salt-dependent B-to-A transition in base pair models of the poly(dG)·poly(dC) duplex, offers two sigmoidal variations of the dielectric constant:

$$\epsilon(r_{ij}) = \epsilon_\infty \left(\frac{\exp\left(\frac{1.8r_{ij}}{r_{mid}}\right)^p + \exp\left(-\left(\frac{1.8r_{ij}}{r_{mid}}\right)^p\right)}{\exp\left(\frac{1.8r_{ij}}{r_{mid}}\right)^p - \exp\left(-\left(\frac{1.8r_{ij}}{r_{mid}}\right)^p\right)} - \left(\frac{r_{mid}}{1.8r_{ij}}\right)^p \right) \qquad (2)$$

The parameter r_{mid} in the above equation is related to the ionic strength of the surrounding environment and is equal to the distance at which $\epsilon = \epsilon_\infty/2$. The coefficient p is set equal to 1 or 2, with the latter form approaching the ϵ_∞ limit more sharply and at shorter distances.

The intrinsic torsional potential V_ϕ associated with a given rotation angle ϕ is obtained using a finite Fourier series with constants chosen to reproduce known torsional barrier heights and gauche/trans energy differences in model compounds.[29] The lone pair interactions of the phosphate are treated with a virtual bond torsional potential of barrier height 1 kcal mol^{-1}.[38]

(39) Altona, C.; Arnott, S.; Danyluk, S. S.; Davies, D. B.; Hruska, F. E.; Klug, A.; Lüdemann, H.-D.; Pullman, B.; Ramachandran, G. N.; Rich, A.; Saenger, W.; Sarma, R. H.; Sundaralingam, M.; Karlson, P.; Kennard, O.; Kim, S.-H.; Sasisekharan, V.; Wilson, H. R. *Eur. J. Biochem.* **1983**, *131*, 9−15.

(40) Gelbin, A.; Schneider, B.; Clowney, L.; Hsieh, S.; Olson, W. K.; Berman, H. M. *J. Am. Chem. Soc.* **1996**, *118*, 519−529.

(41) Chandrasekaran, R.; Arnott, S. In *Landolt-Börnstein Numerical Data and Functional Relationships in Science and Technology, Group VII/1b, Nucleic Acids*; Saenger, W., Ed.; Springer-Verlag: Berlin, 1989; pp 31−170.

(42) Zhurkin, V. B.; Poltev, V. I.; Florent'ev, V. L. *Mol. Biol. (USSR)* **1980**, *14*, 1116−1130.

(43) Poltev, V. I.; Shulyupina, N. V. *J. Biomol. Struct. Dyn.* **1986**, *3*, 739−765.

(44) Pearlman, D. A.; Kim, S. *J. Mol. Biol.* **1990**, *211*, 171−187.

(45) Cheatham, T. E., III; Miller, J. L.; Fox, T.; Darden, T. A.; Kollman, P. A. *J. Am. Chem. Soc.* **1995**, *117*, 4193−4194.

(46) York, D. M.; Yang, W.; Lee, H.; Darden, T.; Pedersen, L. G. *J. Am. Chem. Soc.* **1995**, *117*, 5001−5002.

(47) Manning, G. S. *Quart. Rev. Biophys.* **1978**, 179−246.

(48) Hingerty, B. E.; Ritchie, R. H.; Ferrel, T. L.; Turner, J. E. *Biopolymers* **1985**, *24*, 427−439.

(49) Mazur, J.; Jernigan, R. L. *Biopolymers* **1991**, *31*, 1615−1629.

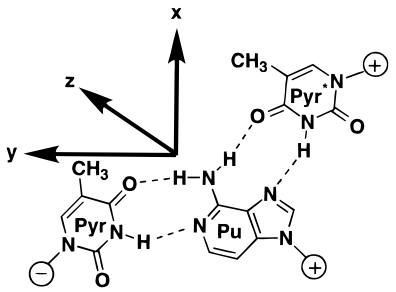

Figure 1. The orthogonal *x*,*y*,*z* reference frame of the pyrimidine·-purine+pyrimidine base triplet. The origin of this reference frame is shifted into the major groove by ~4 Å from the canonical B-DNA duplex. The *y*-axis is roughly parallel to the vector connecting pyrimidine C6 and purine C8 of the T·A Watson−Crick base pair. The starting base triple coordinates (with an inherent propeller twist of −9.2° and a built-in buckle of −1.2° between the T·A base pair) are taken from the X-ray fiber model.[16]

Results

Base Stacking Energies. The intrinsic flexibility of the triplex is estimated from the energies of neighboring base triples. The extra Hoogsteen-linked pyrimidine base (T) is omitted in the duplex calculations. The base positions in the poly(dT)·-poly(dA)+poly(dT) fiber diffraction model are used as the reference state in both computations. A coordinate frame is defined with respect to the starting Watson−Crick base pair plane so that rolling motions (Ro) correspond to rotations about the long axis (*y*-axis) and tilting motions (Tl) to angular changes about the short axis (*x*-axis) of the base pair. The *y*-axis so defined is very nearly parallel to the long axis of the Watson−Crick base pair. The origin of this coordinate system, however, is shifted into the major groove from the base pair origin of the standard B-DNA reference frame. This coordinate frame is described in Figure 1 with the Watson−Crick hydrogen-bonded pyrimidine and purine bases designated respectively by Pyr and Pu and the Hoogsteen-linked pyrimidine base by Pyr*. Successive residues in the reference triplex are generated through a translation of 3.26 Å along the starting base pair normal (i.e., *z*-axis) and a rotation Tw about the same axis.

The nonbonded energies $V_{i,i+1}$ between adjacent base triples, computed at 5° increments in Ro and Tl over the range −30° to +30° and at 2° increments in twist (i.e., the rotation Tw about the vertical axis) from 26° to 36°, are expressed in terms of the residue partition function *z* given by

$$z = \sum_{\mathrm{Tw}}\sum_{\mathrm{Ro}}\sum_{\mathrm{Tl}} \exp(-V_{i,i+1}(\mathrm{Tw},\mathrm{Ro},\mathrm{Tl})/RT) \qquad (3)$$

Here, *R* is the universal gas constant and *T* is the absolute temperature (taken as 298 K). The flexibility of the triplex defined on this basis is appreciably reduced compared to that of the duplex and justifies the treatment of perfectly parallel base planes in our models of backbone-linked triple helixes. The partition function corresponding to the free base triplex, $z_{\mathrm{W}\cdot\mathrm{C+H}} = 2.3$, is roughly one-third that of the duplex, $z_{\mathrm{W}\cdot\mathrm{C}} = 6.4$. The association of a third base through a Hoogsteen arrangement markedly restricts the bending of the chain, leading to nearly a 4-fold increase in the computed persistence length of the triplex (see ref 50 for procedural details). Experimental measurements of triplex persistence lengths, however, are not available. Recent transient electric birefringence measurements of double-helical $dA_n\cdot dT_n$ and merotriplex $\{[A]_{n/2}\cdot/+dT_n\}$ DNAs,[51] nevertheless, demonstrate that the triple-helical structures, in which the single-stranded poly(thymidylate) species folds back upon itself to provide the two polymer strands of the merotriplex formed with the free purine bases, are almost as rigid as their duplex counterparts.

Table 1. Total Number of Monomeric Backbone Linkages of DNA and RNA Triple-Helical Structures at the Polymer Level

				sugar puckering		
strand	linkage	M_1[a]	M_2[a]	*NN*	*EE*	*SS*
		DNA (12-fold)				
Pyr	3′-5′	160	7	0	5	2
Pu	3′-5′	139	14	1	9	4
Pyr*	3′-5′	150	13	4	8	1
		RNA (12-fold)				
Pyr	3′-5′	160	7	2	4	1
Pu	3′-5′	139	17	3	12	2
Pyr*	3′-5′	150	7	2	5	0
		DNA (13-fold)				
Pyr	3′-5′	137	5	0	5	0
Pu	3′-5′	157	7	1	4	2
Pyr*	3′-5′	155	8	0	8	0

[a] M_1 = total number of acceptable covalent linkages; M_2 = number of low-energy linkages (rel energy ≤ 10 kcal mol^{-1}).

Backbone Linkages. The multiple sugar−phosphate backbones that link adjacent bases in the pyrimidine (Pyr), purine (Pu), and Hoogsteen (Pyr*) strands of the triplex have been obtained using both an exhaustive search of conformation space at the dimer level and a more limited polymer modeling scheme. The PyrPyr, PuPu, and Pyr*Pyr* base steps are first considered separately in the searches of acceptable phosphodiester linkages. The preliminary set of backbone conformations (data not shown) fall into five low-energy categories corresponding to the puckering of the sugar rings. Consistent with a number of earlier computational estimates,[28,52,53] the $O_{1'}$-endo conformational combination dominates over all others in the three dinucleotide steps of the DNA mini triplex. Importantly, for all dimer steps mixed $C_{3'}$-endo:$C_{2'}$-endo states occur more frequently than $C_{2'}$-endo:$C_{3'}$-endo sugar puckers. This disproportionality points to possible limitations on mixed sugar puckering states in long triple-helical structures. As a result, all subsequent analyses of triple-helical conformations are focused on monomeric repeating units with identical sugar puckerings in successive residues.

As detailed above, a search of polymer models with identical monomer repeats was undertaken to explore the triplex forming potentials of DNA- and RNA-linked polymer chains. The DNA and RNA polymer backbones connecting each of the three single-stranded steps of the (Pyr = T, Pu = A, Pyr* = T) triple helix are reported in Table 1. The total number of computed polymer solutions (M_1) and the smaller subset of states (M_2) obtained after introducing a 10 kcal mol^{-1} relative energy limit (compared to the lowest energy conformation) for each dimer step are listed respectively in the third and the fourth columns of Table 1. The number of polymer solutions represents only a small fraction of the successfully closed dimer steps for each of the three strands. Further classification of the low-energy structures based on sugar puckering preferences is also reported

(50) Olson, W. K.; Marky, N. L.; Jernigan, R. L.; Zhurkin, V. B. *J. Mol. Biol.* **1993**, *232*, 530−554.
(51) Hagerman, K. R.; Hagerman, P. J. *J. Mol. Biol.* **1996**, *260*, 207−223.
(52) Laughton, C. A.; Neidle, S. *J. Mol. Biol.* **1992**, *223*, 519−529.
(53) Piriou, J. M.; Ketterlé, C.; Gabarro-Arpa, J.; Cognet, J. A. H.; Le Bret, M. *Biophys. Chem.* **1994**, *50*, 323−343.

Table 2. Computed Lowest Energy Helical Conformation States for Pyrimidine (Pyr), and Purine (Pu), and Hoogsteen (Pyr*) Single Strands of the 12-fold Triplex Repeating Units from Table 1

strand	no. of states	*P*	χ ($C_{3'}$	$\frac{\epsilon}{\phi'}$ $O_{3'}$	$\frac{\zeta}{\omega'}$ P	$\frac{\alpha}{\omega}$ $O_{5'}$	$\frac{\beta}{\phi}$ $C_{5'}$	$\frac{\gamma}{\psi}$ $C_{4'}$)	av energy/ nucleotide[a]
				DNA					
Pyr	3	*E*	*a*	*t*	g^-	g^-	*t*	g^+	3.9
Pyr	1	*S*	*a*	*t*	g^-	*t*	g^+	*t*	2.7
Pyr	2	*E*	*a*	*t*	s^-	g^-	*t*	g^+	6.9
Pyr	1	*S*	*a*	*t*	s^-	g^-	*t*	g^+	9.6
Pu	1	*S*	*a*	*t*	g^-	s^-	g^+	*t*	0.0
Pu	2	*S*	*a*	*t*	s^-	g^-	*t*	g^+	4.3
Pu	1	*S*	*ha*	*t*	g^-	g^-	*t*	g^+	5.2
Pu	4	*E*	*a*	*t*	s^-	g^-	*t*	g^+	7.1
Pu	1	*E*	*a*	g^+	g^+	g^+	*t*	*t*	6.9
Pu	3	*E*	*a*	*t*	g^-	g^-	*t*	g^+	8.0
Pu	1	*E*	*a*	s^-	g^-	s^-	s^+	*t*	8.1
Pu	1	*N*	*a*	*t*	g^-	g^-	*t*	g^+	9.9
Pyr*	3	*N*	*a*	*t*	g^-	g^-	*t*	g^+	2.4
Pyr*	6	*E*	*a*	*t*	g^-	g^-	*t*	g^+	5.4
Pyr*	1	*E*	*a*	*t*	g^-	s^-	g^+	*t*	2.9
Pyr*	1	*N*	*a*	g^+	g^+	g^+	g^+	*t*	6.0
Pyr*	1	*E*	*a*	s^-	g^-	*t*	*t*	*t*	6.6
Pyr*	1	*N*	*a*	*t*	s^-	g^-	*t*	g^+	7.4
B-DNA[b]		*S*	*ha*	*t*/g^-	g^-/*t*	g^-	*t*	g^+	
				RNA					
Pyr	2	*E*	*a*	*t*	s^-	g^-	*t*	g^+	1.9
Pyr	1	*S*	*a*	*t*	s^-	g^-	*t*	g^+	1.7
Pyr	1	*E*	*a*	g^-	g^-	g^-	g^+	s^+	4.8
Pyr	1	*E*	*a*	*t*	g^-	g^-	*t*	g^+	4.9
Pyr	1	*N*	*a*	*t*	g^-	g^-	*t*	g^+	6.4
Pyr	1	*N*	*a*	g^-	*t*	g^+	g^-	*t*	6.9
Pu	2	*N*	*a*	*t*	g^-	g^-	*t*	g^+	1.8
Pu	3	*E*	*a*	*t*	g^-	g^-	*t*	g^+	4.9
Pu	4	*E*	*a*	*t*	s^-	g^-	*t*	g^+	7.4
Pu	1	*E*	*a*	s^-	g^-	g^-	g^+	s^+	6.6
Pu	1	*E*	*a*	s^-	g^-	s^-	s^+	s^+	6.9
Pu	1	*E*	*a*	s^-	s^-	s^+	g^-	*t*	7.0
Pu	2	*S*	*a*	*t*	s^-	g^-	*t*	g^+	8.4
Pu	1	*N*	*a*	g^-	g^-	g^-	s^+	s^+	7.3
Pu	1	*E*	*a*	s^-	g^-	g^-	s^+	g^+	7.7
Pu	1	*E*	*a*	s^-	g^-	s^-	s^+	*t*	9.5
Pyr*	1	*N*	*a*	*t*	g^-	g^-	*t*	g^+	0.0
Pyr*	4	*E*	*a*	*t*	g^-	g^-	*t*	g^+	6.4
Pyr*	1	*N*	*a*	g^+	g^+	g^+	*t*	*t*	8.3
Pyr*	1	*E*	*a*	*t*	s^-	g^-	*t*	g^+	9.9
A-DNA[b]		*N*	*a*	*t*	g^-	g^-/*t*	*t*	g^+/*t*	

[a] Average relative energies (in kcal mol^{-1}) computed with respect to the lowest energy conformation of a given class taken as zero. [b] Values based on the survey of crystal structures reported in ref 59.

in Table 1. The *EE* states with unusual $O_{1'}$-endo sugar puckering once more dominate all steps. As noted above, similar sugar puckering preferences have been found in molecular dynamics simulations of model triple helixes.[28,52,53] However, it is well-known that $O_{1'}$-endo sugar conformations occur only rarely in high-resolution crystal structures of low molecular weight nucleic acid analogues[40] and in oligonucleotide crystal structures[24] and are intrinsically of high energy.[29] Table 1 further reveals that the deoxyribose sugars of the purine strand, in agreement with solution data,[17,54] have a slightly greater tendency to adopt $C_{2'}$-endo (*S*) over $C_{3'}$-endo (*N*) puckering in the regular triplex. The sugar puckering preferences of the RNA backbone, by contrast, include large numbers of $O_{1'}$-endo (*E*) states and more examples of $C_{3'}$-endo (*N*) than of $C_{2'}$-endo (*S*) sugar puckers.

(54) Rajagopal, P.; Feigon, J. *Biochemistry* **1989**, *28*, 7859−7870.

Also reported in Table 1 are the number of occurrences of low-energy states for the three single strands in a 13-fold DNA triplex. The Pyr and Pyr* strands of these monomers adopt the energetically less favored $O_{1'}$-endo (*EE*) sugar puckering state exclusively, whereas the purine strand shows some additional tendency for $C_{2'}$-endo (*SS*) and $C_{3'}$-endo (*NN*) puckering. These structures are quite different from the published models based on X-ray fiber diffraction patterns of single crystals of 13-fold triple-helical DNA,[25] in which the $C_{2'}$-endo family of sugar puckering is proposed for all the three single strands.

The computed low energy helical conformations for the Pyr, Pu, and Pyr* strands in the 12-fold triple helixes are further described in Table 2. The chain backbone torsions are classified into six ranges corresponding to cis ($c = 0° \pm 20°$), *gauche*$^\pm$ ($g^\pm = \pm 60° \pm 40°$), *skew*$^\pm$ ($s^\pm = \pm 120° \pm 20°$), and trans ($t = 180° \pm 40°$) arrangements. The glycosyl conformations are

Table 3. Minimum Long-Range Nonbonded Energies (in kcal mol^{-1}) under Different Dielectric Treatments and Groove Widths (in Å) of Regular 12-fold Triple Helixes Composed of 16-mer (T·A+T) DNA and RNA Single Strands

	dielectric treatment					groove widths		
				eq 2				
strands[a] (Pyr·Pu+Pyr*)	ϵ_∞	DH	eq 1	(p=1)	(p=2)	Pyr···Pyr*	Pyr*···Pu	Pu···Pyr (minor groove)
D_S·D_S+D_S	143	139	−475	−75	−274	15.7	8.0	10.7
D_S·D_S+R_N	188	184	−319	12	−160	12.7	10.7	10.7
D_S·R_N+D_S	174	170	−279	17	−139	15.7	4.9	13.8
D_S·R_N+R_N	226	221	−121	110	−20	12.7	7.2	13.8
R_N·D_S+D_S	446	442	−61	269	99	12.5	8.0	13.5
R_N·D_S+R_N	491	486	95	357	214	9.2	10.7	13.5
R_N·R_N+D_S	477	472	136	362	235	12.5	4.9	16.3
R_N·R_N+R_N	530	523	295	455	354	9.2	7.2	16.3

[a] D = DNA; R = RNA; S = $C_{2'}$-endo; N = $C_{3'}$-endo.

divided into four angular ranges where the sugar-base linkage is anti ($a = 30° \pm 45°$), high anti ($ha = 120° \pm 45°$), syn ($s = 210° \pm 45°$), or high syn ($hs = 300° \pm 45°$). Chain backbone torsions are described with respect to a 0° planar cis reference state and glycosyl torsions are defined with respect to cis arrangements of the $O_{1'}-C_{1'}-N_1-C_6$ (pyrimidine) and $O_{1'}-C_{1'}-N_9-C_8$ (purine) atomic sequences. Also, reported in Table 2 are the average relative energies per nucleotide for each local conformational state and the number of conformations of a given type. A number of sterically unfavorable states with unusual E ($O_{1'}$-endo) sugar puckerings are evident in the lowest energy models in the table. Notably, in all cases the exocyclic $C_{5'}-C_{4'}$ (γ) torsion adopts favorable t or g^+ states. Similarly, the phosphodiester ($\zeta\alpha$) conformations in the lowest energy structures are limited to a narrow range of (g^- or s^-) states. The glycosyl torsion (χ) is uniformly anti.

Regular Polymer Models. To understand the potential helix-forming tendencies of the various monomer building blocks, we have generated DNA and RNA 16-mers and determined the total (intra- plus intermolecular) energies of the different hybrid triple helixes. Only the lowest energy states corresponding to each base pair step with $C_{2'}$-endo (S) (in the case of DNA) and $C_{3'}$-endo (N) (for RNA) sugar puckerings are included in the hybrid structures. This is consistent with the decided preference of $C_{2'}$-endo sugar puckerings in B-DNA and $C_{3'}$-endo sugar puckerings in RNA observed in numerous oligonucleotide single-crystal structures.[24,40] The single strands forming part of the various triplex structures are identified in Table 3 by the backbone chemistry, D (DNA) or R (RNA), followed by a subscript, S ($C_{2'}$-endo) or N ($C_{3'}$-endo), designating the sugar puckering. The absolute values of the total potential energies corresponding to the triple-helical hybrids—D_S·D_S+D_S, D_S·D_S+R_N, D_S·R_N+D_S, etc.—are reported in the Table 3. These energies include electrostatic contributions based on the five different dielectric treatments described above. The groove widths—Pyr···Pyr*, Pyr*···Pu, and Pu···Pyr (i.e., minor groove)—associated with the different triplexes are also listed in the table. These values correspond to the shortest distances across the ribbon-like virtual bond pathways connecting successive phosphorus (P) atoms on the edges of the specified grooves.[55] As evident from the table, the Pyr*···Pu groove shows the greatest fluctuations (4.9−10.7 Å) in the low-energy complexes, increasing in width (8.0−10.7 Å) when the purine strand is DNA but shrinking (4.9−7.2 Å) when the purine backbone is RNA. A superposed stereo representation of two of the lowest energy triple-helical complexes (D_S·D_S+D_S and D_S·R_N+D_S) is illustrated in Figure 2. Strands are color-coded according to base identity with the Watson−Crick pyrimidine strand red and the Hoogsteen-bonded strand green. The purine D_S strand of the D_S·D_S+D_S triplex is shown in blue and that of the D_S·R_N+D_S triplex in gray. The narrow Pyr*···Pu groove of the D_S·D_S+D_S triplex (i.e., the space between the green and blue strands) is readily apparent from the figure. It is also clear from the images that the introduction of an RNA purine (R_N) strand reduces the width of the Pyr*···Pu groove still further (compare the spacing between green and blue versus green and gray strands).

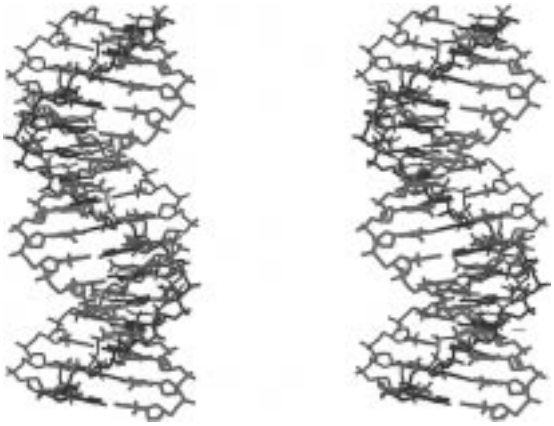

Figure 2. Superposed stereo diagram illustrating the lowest energy triple helical conformation of D_S·D_S+D_S and D_S·R_N+D_S triplexes. The pyrimidine, purine, and Hoogsteen DNA strands are colored respectively in red, blue, and green, while the RNA purine strand R_N is shown in gray.

On the basis of the nonbonded energies reported in Table 3, the all-D triplex is predicted to be highly stable while the triple-helical structure with only RNA strands is consistently least stable. The energies computed with the Hingerty[48] and Mazur-Jernigan[49] dielectric treatments (eqs 1 and 2) reveal the following overall hierarchy of stabilities: D_S·D_S+D_S > D_S·D_S+R_N > D_S·R_N+D_S > D_S·R_N+R_N > R_N·D_S+D_S > R_N·D_S+R_N > R_N·R_N+D_S > R_N·R_N+R_N. The order changes slightly when the rankings are based on energies computed with the Debye−Hückel and $\epsilon_\infty = 78.3$ electrostatic treatments. This ordering of triple helical energies also agrees qualitatively with trends found from gel electrophoresis studies on similar complexes[14] and from calorimetric investigations of D·D+D and D·D+R triplexes.[13] According to both the experimental observations and the computed energies, single-stranded DNA and RNA can easily bind to double-stranded Watson−Crick DNA and form a stable triple-helical complex.

Experimental studies[11,14,15] indicate that the D·R+D and R·R+D complexes are the least stable among all DNA, RNA, and hybrid triple-helical structures. However, on the basis of

(55) Srinivasan, A. R.; Olson, W. K. *Biochemistry* **1994**, *33*, 9389−9404.

the present energetic criteria, the D·R+D triplex structure is predicted to be lower in energy than most other strand combinations. This result is, nevertheless, consistent with the recent observation of a stable D·R+D poly(dT)·poly(rA)+poly(dT) triplex in the presence of selected nucleic acid binding ligands[56] (see below). It is important to note that none of the available experimental data provide information on the sugar puckering in the three-stranded complexes.

Discussion

The variety of DNA, RNA, and hybrid DNA/RNA triple-helical structures generated here point to the extent to which sugar puckering may contribute to the stability of these complexes. The furanose puckering determines the structural character of the triplex as a whole, defining both the groove widths (Figure 2) and the long-range interactions of the negatively charged sugar−phosphate backbone (Table 3). The computationally predicted structures reflect a balance between the intrinsic energy of pseudorotation and the accompanying interactions with other parts of the polymer. The energy treatment used here, however, is too crude to predict the outcome of this tug-of-war between local and long-range forces. Further information from solid-state and solution studies must be gathered before the relative energetics of the various triplex schemes can be well understood.

Simple assessment of the nonbonded interactions of neighboring base triplets clearly shows how the introduction of a Hoogsteen-bonded third base restricts the mobility of the triple strand as a whole. The rolling and tilting motions of unlinked hydrogen-bonded bases, studied over a range of helical twist values (26°−36°), are considerably reduced in the free base triplex compared to the corresponding pseudo (unlinked) double helix. This restriction may be a factor controlling the overall behavior of triple-helical nucleic acid structures.

A useful outcome of the current work is the capability to model hybrid DNA and RNA triple-helical structures in a wide range of conformations. The relative energetics of the various models, differing mainly in the backbone torsion angles, help to make sense of the observed stabilities of hybrid structures such as the DNA·RNA+DNA complex. This triplex structure, found to be highly unstable in a number of experiments,[11,14,15] has recently been shown to occur in the presence of certain nucleic acid binding ligands (e.g., berenil, DAPI, ethidium, netropsin).[56] The current calculations predict this structure to be relatively low in energy compared to other hybrid triplexes. The conformation of the Hoogsteen strand, however, is somewhat unusual with backbone and glycosyl angles altered from the ideal B-form structure, $\alpha\beta\gamma = tg^-g^+$, $\chi = a$ in the model triplex versus $\alpha\beta\gamma = g^-tg^+$, $\chi = ha$ in B-DNA. Furthermore, the introduction of standard B-DNA geometry in the third strand raises the energy of the molecular complex. The drug-enhanced stability of the DNA·RNA+DNA triplex may thus reflect this conformational transition, with the ligand facilitating changes in Hoogsteen strand geometry not possible in the ordinary three-stranded complex. Drug-induced structural perturbations are well-known to occur in single-crystal X-ray studies of oligonucleotide duplexes complexed with groove binding ligands.[2] The composite data suggest that triplex stabilities are governed not only by the chemical nature of the single strands (DNA or RNA) but also by the backbone conformations of the constituent oligomers and that a ligand-induced change in the backbone conformation can transform an otherwise unstable structure to a stable one.

The overall stabilities of the different triplexes predicted in the current study fall in the following order regardless of electrostatic treatment: $D_S{\cdot}D_S{+}D_S > D_S{\cdot}D_S{+}R_N > D_S{\cdot}R_N{+}D_S > D_S{\cdot}R_N{+}R_N > R_N{\cdot}D_S{+}D_S > R_N{\cdot}D_S{+}R_N > R_N{\cdot}R_N{+}R_N$. (The ranking of the $R_N{\cdot}R_N{+}D_S$ triplex, which is not observed experimentally, is more favored when $\epsilon = \epsilon_\infty$ or when a Debye−Hückel term is employed than when the sigmoidal forms are used). By contrast, the experimentally derived stabilities follow three rankings: (1) R·D+R > D·D+R > R·R+R > R·D+D > D·D+D > D·R+R according to spectroscopically derived (ultraviolet) temperature-dependent free energies;[11,12] (2) D·D+R > R·D+R > D·D+D > D·R+R = R·D+D = R·R+R obtained from UV absorption spectrophotometry and molecular modeling;[15] and (3) D·D+D > D·D+R > R·D+R > R·D+D > D·R+R > R·R+R based on electrophoresis measurements.[14] Direct calorimetric rankings of the D·D+D and D·D+R complexes[13] agree more closely with the binding constants derived from the gel study,[14] but concur with the ultraviolet spectroscopic analysis[15] in showing that the triplex to duplex melting is entropy driven. The energies of the hybrid complexes computed here match the gel electrophoresis data[14] qualitatively, although correspondence between the precise order of observed stabilities and the theoretical rankings is imperfect. The calculations invert the order of two of the observed states (R·D+R and D·R+D) and, as noted above, predict the occurrence of the D·R+D triplex in the absence of stabilizing ligands. Otherwise there is a 1:1 agreement with the gel electrophoresis data.[14] It is important to note that the current calculations provide no insight into "melting processes"; this level of structural understanding can only come from more elaborate simulation methods (e.g., free energy perturbation studies[57,58]).

The triple-helical models presented here illustrate some of the more likely ways in which DNA and RNA chains may associate with one another. These idealized poly(dT)·poly(dA)+poly(dT) structures are useful starting points for more detailed molecular dynamics simulations incorporating explicit solvent atoms and ions. Our model building procedure offers a way to generate and assess the relative importance of the wide range of conformations that a nucleic acid might adopt. Molecular dynamics simulations, by contrast, do not sample states significantly different from the assumed starting structure. Here, we have a way to choose better starting structures for such state-of-the-art simulations incorporating sequence effects. An obvious next step is to extend the present calculations to charged base triples ($G{\cdot}C{+}C^+$), which are needed for modeling heterogeneous triple-helical complexes. The residual charges on cytosine will have no effect on the sterically allowed backbones identified in this work but may change the relative ordering of DNA and RNA triplexes. Our approach can also be used to design various nucleic acid binding ligands (DNA mimics) and to visualize their structures as outlined in the paper that follows.[59] While the relative placement of adjacent base triples has been kept fixed in this study, repositioning the base triple proves to be important in modeling the third strand binding of DNA mimics. The variation of base stacking parameters

(56) Pilch, D. S.; Breslauer, K. J. *Proc. Natl. Acad. Sci. U.S.A.* **1994**, *91*, 9332−9336.

(57) Pearlman, D. A.; Kollman, P. A. In *Computer Simulation of Biomolecular Systems*; van Gunsteren, W. F., Weiner, P. K., Eds.; ESCOM: Leiden, 1989; Vol. 1, pp 101−119.

(58) Hausheer, F. H.; Singh, U. C.; Saxe, J. D.; Flory, J. P.; Tufto, K. B. *J. Am. Chem. Soc.* **1992**, *114*, 5356−5362.

(59) Srinivasan, A. R.; Olson, W. K. **1998**, *120*, 492−499.

from canonical geometry also disrupts the DNA/RNA triplex backbone (see reference 59).

Acknowledgment. Sponsorship of this research by the U.S. Public Health Service under research grant GM-20861 is gratefully acknowledged. We thank Dr. Daniel Pilch and Dr. Jens Völker for many helpful discussions; Dr. Bryan M. Craven and Dr. V. I. Poltev for detailed information about the atomic charges and potential functions used in this study; Professor B. Montgomery Pettitt for insight into force field effects on molecular simulations; and Professor Donald M. Crothers for providing a copy of the Ph.D. thesis of Dr. Richard M. Roberts. Computations were performed at the Rutgers Center for Computational Chemistry. Stereo diagrams were generated using a PostScript graphics program developed in this laboratory.

Supporting Information Available: Table of atomic coordinates for Figure 2 (30 pages). See any current masthead page for ordering information and Web access instructions.

JA972720K